

Research Article

Experimental Study on Shear Behavior and Acoustic Emission Characteristics of Nonpersistent Joints

Yujing Jiang,^{1,2,3} Yongqiang Chen,^{1,2} Xianzhen Cheng,^{1,2} Hengjie Luan^{1,2} ,
Sunhao Zhang,^{1,2} Qizheng Zhao,² and Wei Han³ 

¹State Key Laboratory of Mining Disaster Prevention and Control Cofounded by Shandong Province and the Ministry of Science and Technology, Shandong University of Science and Technology, Qingdao 266590, China

²College of Energy and Mining Engineering, Shandong University of Science and Technology, Qingdao 266590, China

³Graduate School of Engineering, Nagasaki University, Nagasaki 852-8521, Japan

Correspondence should be addressed to Hengjie Luan; luanjie0330@126.com

Received 14 August 2020; Revised 14 September 2020; Accepted 6 November 2020; Published 21 December 2020

Academic Editor: Shengnan Nancy Chen

Copyright © 2020 Yujing Jiang et al. This is an open access article distributed under the Creative Commons Attribution License, which permits unrestricted use, distribution, and reproduction in any medium, provided the original work is properly cited.

The shear behavior of rock discontinuities controls the stability of rock masses to a great extent. In this paper, laboratory shear tests were performed on rock-like materials with different cracks to study the effect of nonpersistent joints on the shear behavior of rock masses. The results show that the variation trends of the shear stress-displacement curves of specimens with different cracks are generally similar and have the same stage characteristics. When the crack length is relatively short, the elastic stage is prolonged, the peak shear strength decreases, and the shear displacement corresponding to the peak shear strength and the residual shear strength increases with the increase of the crack length. When the crack length is relatively long, the elastic stage is shortened, the peak shear strength decreases, and the shear displacement corresponding to the peak shear strength increases with the increase of the crack length. The peak shear stress gradually decreases with the increase of the crack length. The shear strength of the specimens with unilateral cracks is much higher than that of the specimens with bilateral cracks. The shear strength of the specimens is affected not only by the crack length but also by the crack distribution. The acoustic emission (AE) count peak occurs when the shear stress drops sharply and has an inverse “S”-type variation trend with the increase of the crack length. The inclination angle of the fracture decreases, the roughness of the fracture surface decreases, and the proportion of the wear area on the fracture surface increases gradually with the increase of the crack length. The AE source decreases with the increase of the crack length, and their locations are obviously asymmetric. This work can greatly contribute to the insight into the shear failure mechanism of rock discontinuities with nonpersistent joints.

1. Introduction

Jointed rock mass is a kind of complex engineering medium widely encountered in water conservancy, transportation, mining, foundation, oil exploitation, and other rock projects, which plays an important role in the stability of the project [1, 2]. Rock discontinuities of varying styles, such as joints, beddings, and faults, are commonly encountered in jointed rock masses [3]. The failure characteristics of rock masses are influenced not only by rock mass types but also by rock discontinuities more seriously [4, 5]. Shear failure caused by rock discontinuities is one of the most common failure forms of various types of rock engineering; the shear failure charac-

teristics of rock discontinuities play an indispensable role in the safety and stability of rock engineering [6]. Due to the limitation of rock mass testing technology, it is difficult to evaluate the shear characteristics of discontinuous rock masses in situ, so most of them are studied by experiment. For example, Shrivastava and Rao performed laboratory tests on the modeled infilled rock joint having different types of joint roughness at various initial normal stresses to study the effect of infill on the shear behavior of rock joints [7]. Mehrishal et al. conducted an experimental study on normal stress and shear rate dependency of basic friction coefficient in dry and wet limestone joints [8]. Niktabar and Rao carried out a series of tests on cast regular and irregular jointed



FIGURE 1: Rock-like specimens with different cracks: (a) specimens with unilateral crack; (b) specimen without crack and specimens with bilateral crack.

samples using cyclic shear testing to study the effect of irregular asperities on shear behavior of rock joints [9]. Cui used direct shear tests to investigate the shear behavior of continuous planar joints, stepped joints, and discontinuous open joints [10]. Singh and Basu performed shear tests to compare the shear behavior of “real” natural rock discontinuities and their replicas [11]. Jiang et al. presented a method for characterizing the shear damage of a natural rock joint, which can overcome the “bottleneck” difficulty in insufficient joint specimens with the same natural surface morphologies for experimental study [12]. Some insightful understanding of the shear behavior of rock discontinuities has been obtained through previous studies. The joints can be divided into persistent joints and nonpersistent joints in the engineering site. However, as one particular type of joints, nonpersistent joints have been given less consideration [13]. Compared with the persistent joints, the stress and failure characteristics of the nonpersistent joints have great changes. The influencing factors are more complex, and the hidden danger of engineering safety is greater [14, 15]. Therefore, it is of great engineering value to study the shear mechanical behavior of the nonpersistent joints.

Acoustic emission (AE) activity is highly contrasted with the damage evolution of rock materials, so AE test data were often used to characterize the fracture properties of rock materials in various experiments [16, 17]. Rodríguez et al. carried out compression tests for the characterization of the cracking pattern according to AE parameters, three-dimensional localization of the AE sources, and petrographic analysis [18]. Li et al. made major effort to characterize evolution of the spatial correlation length of AE events, spatial correlation of stress fields, and stress transferring processes [19]. Liu et al. applied AE technique and moment tensor analysis to study the behavior of coarse-grained granite samples under uniaxial compression [20]. Meng et al. carried out shear tests on tensile joints to study the shear behaviors and the changes in the AEs that occurred during shear failure under different normal stresses [21]. However, there are few studies on the mechanical properties, AE characteristics, and failure characteristics during shear failure of rock materials containing nonpersistent joints.

In this paper, the jointed rock samples with cracks at one end of the samples and with cracks at two ends of the samples (the connectivity of these samples is different) are prefabricated firstly. Secondly, the direct shear test and AE monitoring are carried out for these samples. Finally, the influence of

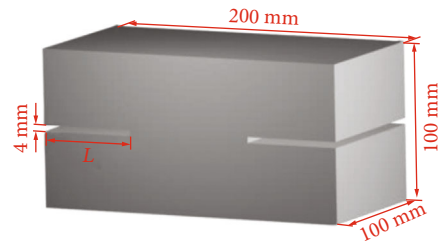


FIGURE 2: Specimen dimension schematic diagram (L : crack length).

the nonpersistent joints on the shear behavior and AE characteristics of the jointed rock mass are discussed. The research results are helpful to further understand the shear instability mechanism of the jointed rock mass and have certain significance for the safety construction and stable operation of rock mass engineering.

2. Experimental Methods

Laboratory shear tests were carried out to study the shear behavior of rock discontinuities with various geometries of cracks.

2.1. Specimen Preparation. The specimens used in the test include a specimen without crack; specimens with unilateral cracks of 2 cm, 4 cm, 6 cm, 8 cm, and 10 cm; and specimens with bilateral cracks of 0 cm, 2 cm, 4 cm, and 6 cm, as shown in Figure 1. Cracks were achieved by hydraulic cutting of complete specimens. The dimensions of all specimens used in the shear tests are 200 mm \times 100 mm \times 100 mm, and the thickness of cracks is 4 mm, as shown in Figure 2. They were made of mixtures of white cement, fine sand, water, and water reducer with weight ratios of 1 : 1 : 0.3 : 0.005, respectively. The main mechanical parameters, such as Young’s modulus, Poisson’s ratio, uniaxial compression strength (UCS), cohesion, and peak friction angle, were 10.35 GPa, 0.166, 41.80 MPa, 8.78 MPa, and 44.01°, respectively [22].

2.2. Experimental Setup. The direct shear test under constant normal load (CNL) conditions were performed using a JAW-600 coupled shear-flow machine (Figure 3(a)) which is developed by Shandong University of Science and Technology [23]. The shear and normal loads are applied using hydraulic actuators equipped with servo valves. Furthermore, the machine has a design capacity of 600 kN in both the shear (horizontal) and normal (vertical) directions and can test

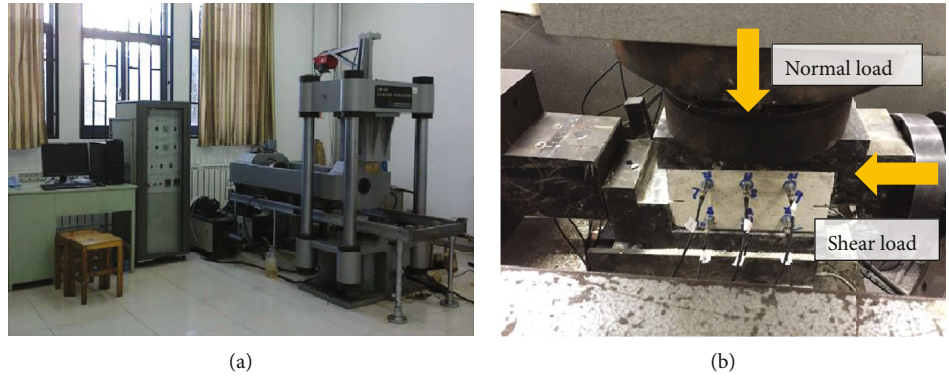


FIGURE 3: Arrangement of the shear test: (a) shear test system; (b) loading unit.

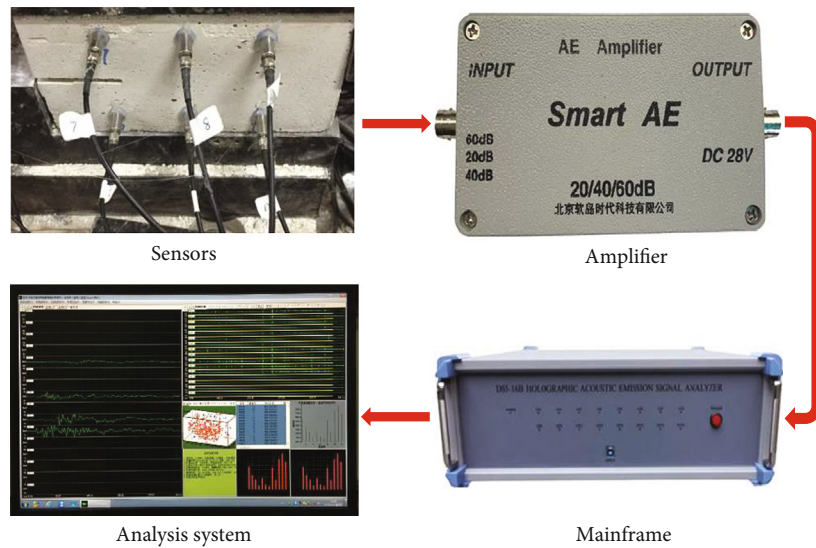


FIGURE 4: DS5-16B AE monitoring system.

for both artificial and natural discontinuities. The shear and normal displacements are measured using linear variable differential transformers (LVDTs). A maximum shear displacement of 25 mm can be obtained. When the joint roughness coefficient is constant, the shear strength of the rock is linearly related to the normal stress acting on the joint surface [24]. Hence, the normal stress is uniformly selected as 1 MPa, which is not taken as an important factor, and the shear rate is chosen as the static limit value of 0.01 mm/s. In the test, the normal load is first applied to a predetermined value and kept constant until the end of the test, and then the shear load is applied. The normal load and shear load are controlled by force and displacement, respectively [25].

The AE characteristics of the rock-like joints were also monitored by a DS5-16B Acoustic Emission System, as shown in Figure 4. Here, 12 sensors were arranged symmetrically on the two free sides which were perpendicular to the shear direction of the sample. The main maximum value of the AE analysis system was set as 40 dB, and the threshold was set as 45 dB. Before the test, an 0.5 mm HB pencil lead was used for the lead breaking test to determine the coupling quality of the sensors. After that, the surface where the sen-

sors were located in was properly polished, and an appropriate amount of coupling agent was applied between the sensors and the sample to ensure better contact [22].

3. Results and Discussion

3.1. Deformation and Strength Characteristics. The shear stress-displacement curves of specimens with different unilateral cracks are shown in Figure 5(a). It can be seen that the variation trends of the shear stress-displacement curves are generally similar and have the same stage characteristics, which can be divided into four stages: compaction stage, elastic stage, unstable failure stage, and residual strength stage. When the crack length is relatively short (0 cm, 2 cm, and 4 cm), with the increase of crack length, the elastic stage is prolonged, the peak shear strength decreases gradually, the shear displacement corresponding to peak shear strength increases gradually, and the residual shear strength also increases gradually. When the crack length is relatively long (6 cm, 8 cm, and 10 cm), with the increase of the crack length, the elastic stage is shortened, the peak shear strength decreases gradually, the shear displacement corresponding

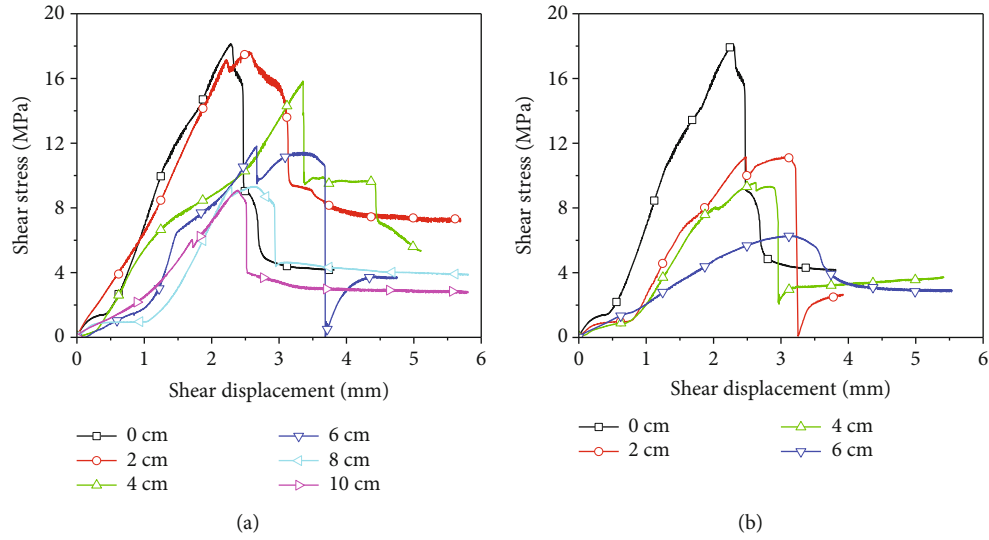


FIGURE 5: Curves of shear stress with respect to displacement of specimens with different cracks: (a) unilateral crack; (b) bilateral crack.

TABLE 1: Peak shear strength of specimens with different cracks.

Crack length (cm)	Unilateral crack						Bilateral crack		
	0	2	4	6	8	10	2	4	6
Shear stress (MPa)	18.15	17.65	15.84	11.82	9.33	9.10	11.17	9.58	6.28

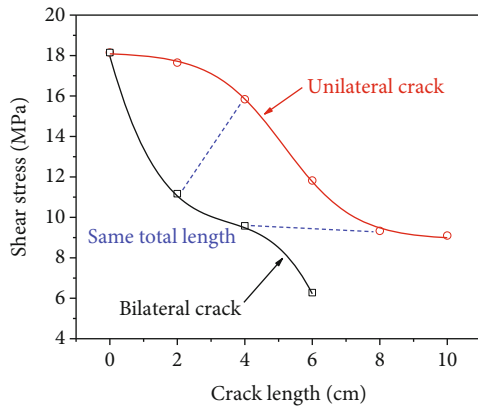


FIGURE 6: Fitting curves of peak shear stress of specimens with different cracks.

to the peak shear strength increases gradually but still lags behind the specimen with no crack, and the residual shear strength decreases gradually.

The shear stress-displacement curves of specimens with different bilateral cracks are shown in Figure 5(b). The phase characteristics of the curves are similar to that of specimens with different unilateral cracks. When the crack length increases from 0 cm to 6 cm, the elastic stage is prolonged and Young's modulus decreases gradually. The peak shear strength decreases gradually, and the shear displacement corresponding to peak shear strength increases gradually. In addition, when the length of the bilateral crack reaches a cer-

tain extent, the postpeak softening characteristics of the specimens are no longer obvious.

3.2. Peak Shear Strength Characteristics. Table 1 lists the measured peak shear strength values of direct shear tests for the two groups of specimens with different cracks. The relationships between peak shear strength, crack location, and length are presented in Figure 6.

As can be seen from Table 1 and Figure 6, the peak shear stresses of two kinds of specimens both gradually decrease with the increase of the crack length. However, the decrease range of the peak shear stress of the specimens with a unilateral crack is first increased and then decreased, while that of specimens with bilateral cracks is first decreased and then increased. Meanwhile, the shear strengths of the specimens with unilateral cracks are much higher than those of the specimens with bilateral cracks. With the increase of the crack length, the strength curves of specimens with unilateral cracks showed an inverse "S" type, while those of specimens with bilateral cracks showed a decentered "S" type.

When the crack length of the specimen with unilateral cracks is no more than 2 cm, it has little impact on the strength of the specimen, and the peak shear strength slowly decreases to 17.65 MPa; when the crack length increases to 8 cm, it has a significant impact on the strength of the specimen under the influence of the length effect, and the shear strength drops sharply to 9.33 MPa; and when the crack length continues to increase to 10 cm, the length effect weakens and the shear strength slightly decreases to 9.10 MPa. Meanwhile, by fitting the shear strengths of the specimen with unilateral cracks with different crack lengths,

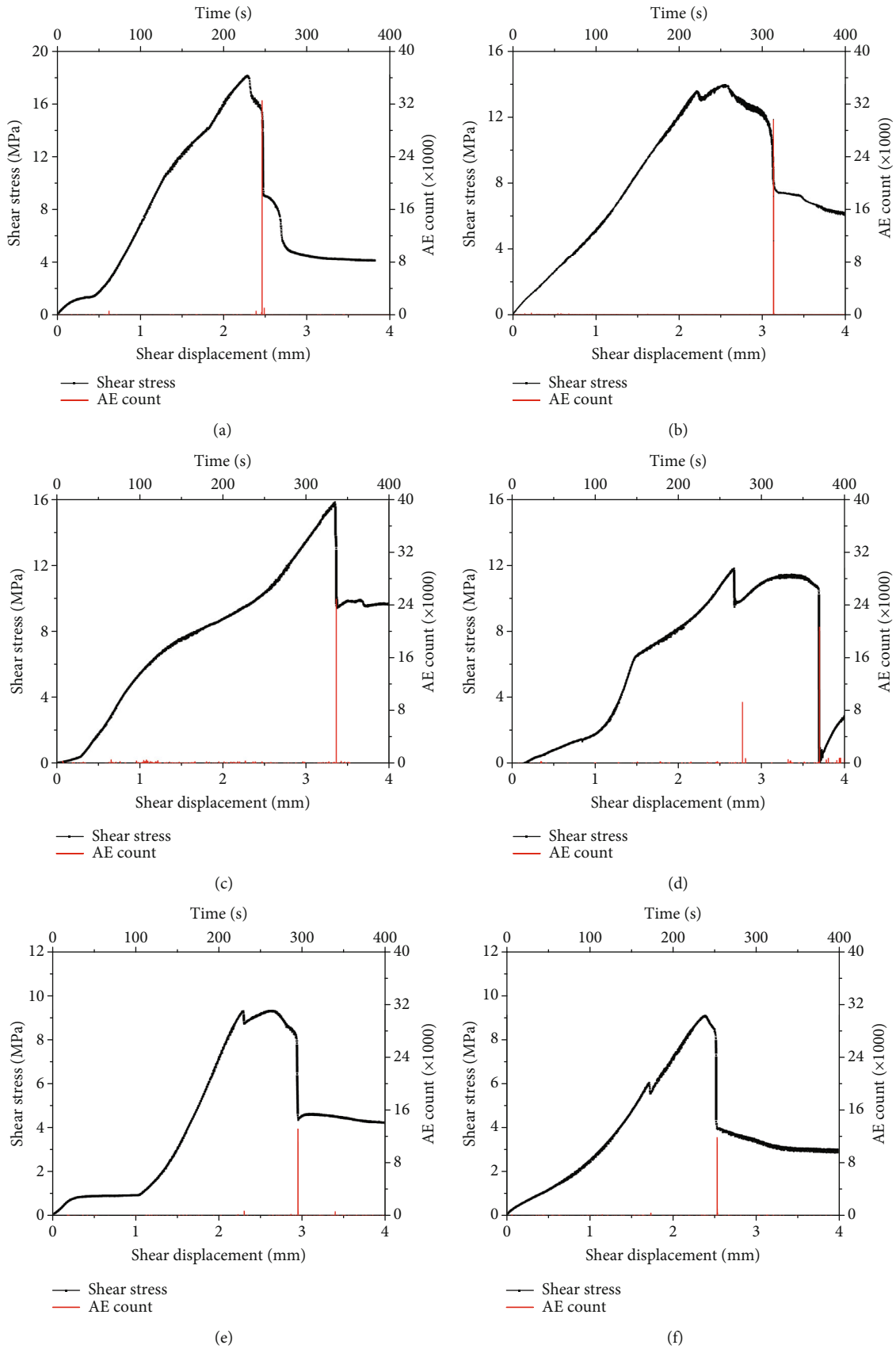


FIGURE 7: The cumulative AE events and shear stress with shear displacement of specimens with unilateral crack of different lengths: (a) 0 cm; (b) 2 cm; (c) 4 cm; (d) 6 cm; (e) 8 cm; (f) 10 cm.

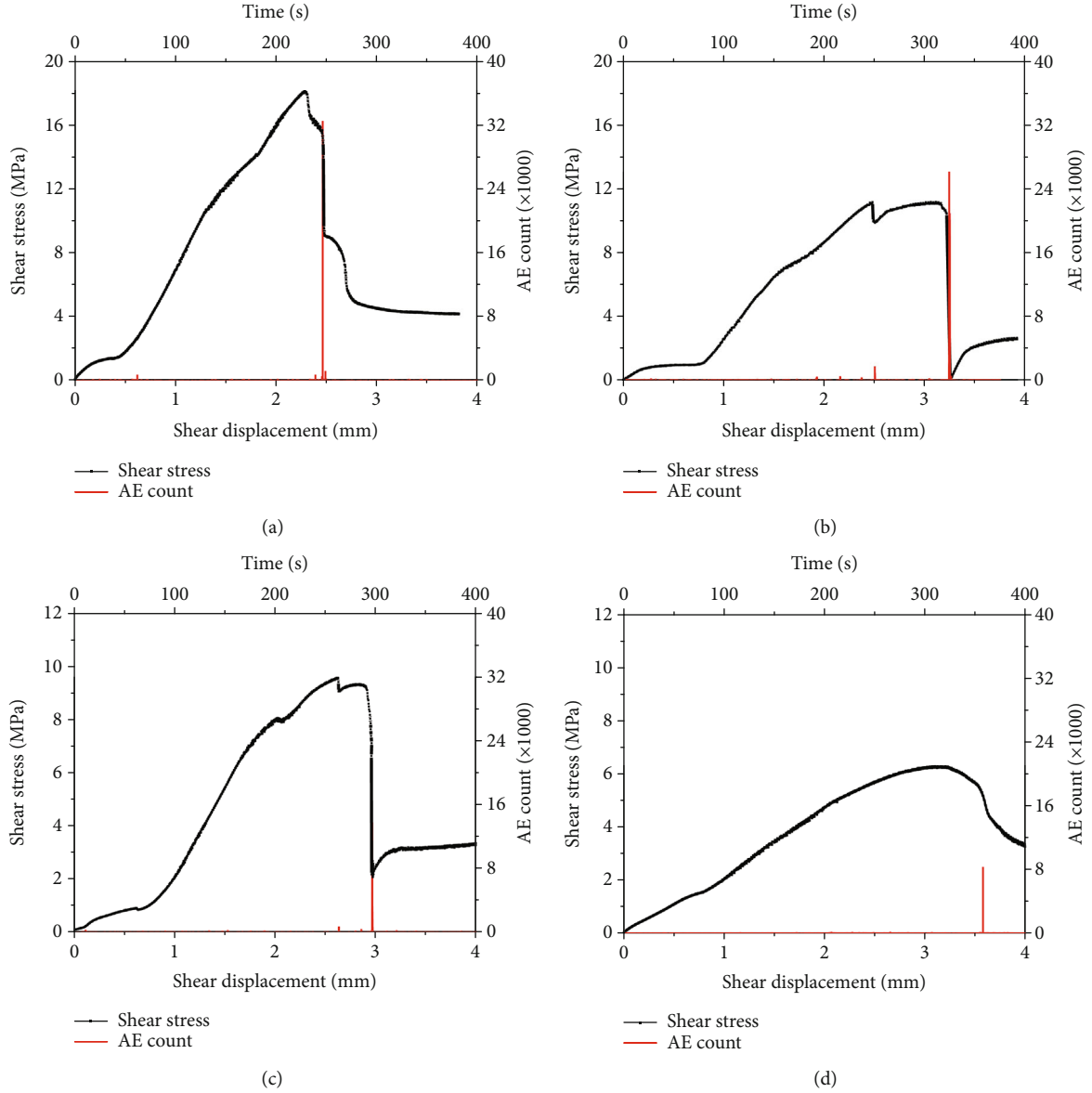


FIGURE 8: The cumulative AE events and shear stress with shear displacement of specimens with bilateral crack of different lengths: (a) 0 cm; (b) 2 cm; (c) 4 cm; (d) 6 cm.

a negative exponential fitting relation with fitting coefficient of 0.9986 can be obtained, as shown:

$$y = \frac{(18.15 - 8.90)}{1 + e^{(x-5.16)/1.05}} + 8.90, R^2 = 0.9986. \quad (1)$$

When the crack length of the specimen with bilateral cracks is 2 cm, it significantly affected the shear strength of the specimen, which dropped sharply to 11.17 MPa; when the bilateral crack length increases to 4 cm, the length effect weakens, and the shear strength slowly decreased to 9.58 MPa; and when the bilateral crack length continues to increase to 6 cm, the length effect is significantly increased again, and the shear strength rapidly decreases to 6.28 MPa. Meanwhile, by fitting the shear strengths of the specimen with bilateral cracks with different crack lengths, polynomial

fitting relation with a fitting coefficient of 0.9992 can be obtained, as shown:

$$y = 17.97 - 5.96x + 1.55x^2 - 0.15x^3, R^2 = 0.9992. \quad (2)$$

In addition, when the total lengths of cracks on the specimens are the same, the shear strengths of the two kinds of specimens are not the same. For example, when the unilateral crack length is 4 cm and the bilateral crack is 2 cm, the shear strength of the specimen with the unilateral crack is much greater than that of the specimen with the bilateral crack. When the unilateral crack length is 8 cm and the bilateral crack is 4 cm, there is little difference in shear strength between the two kinds of specimens. This shows that the shear strength of the specimen is affected not only by the crack length but also by the crack distribution. Moreover,

TABLE 2: Peak value of AE count of rock specimens with different cracks.

Crack length (cm)	Unilateral crack					Bilateral crack			
	0	2	4	6	8	10	2	4	6
AE count peak	32567	29960	24958	20739	13226	11950	26159	13734	8356

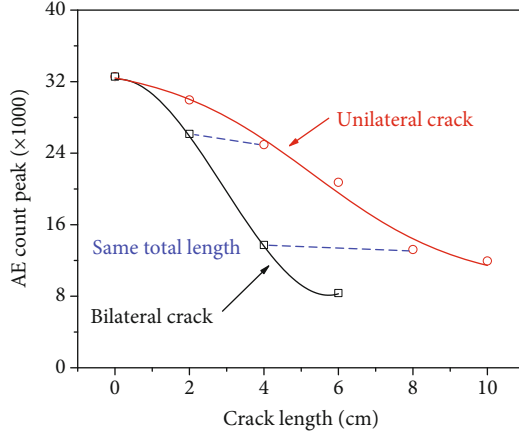


FIGURE 9: Fitting curves of peak value of AE count of specimens with different cracks.

the influence of the distribution on the shear strength of specimens is more obvious when the total crack length is small; the influence is not obvious when the total crack length is large.

3.3. Acoustic Emission Characteristics. We used on-time acoustic emission (AE) to monitor microbreak events and their positions for granite joints during direct shear testing. Then, we analyzed the microsheading behaviors of the non-persistent joints according to the AE events and break localization obtained via AE.

Figures 7 and 8 show the cumulative AE events and shear stress with shear displacement of specimens with different unilateral cracks and bilateral cracks, respectively. It can be seen that the AE count peak of specimens with different crack distributions occurs when the shear stress drops sharply. The AE counts will also have a smaller peak value when the shear stress decreases slightly, and the AE counts at other times are not obvious relative to the peak time. This indicates that the failure and instability of the specimen occurs in an instant, and the energy accumulated in the early loading process is quickly released at the moment of failure and is accompanied by a large number of transient elastic waves. Hence, a strong AE phenomenon is generated. Loud noise was generated when the specimen with a small crack length is destroyed in the test, which further confirms that the specimen will release a large amount of energy at the moment of failure.

Table 2 shows AE count peaks of specimens with different crack distributions. Meanwhile, by fitting the AE count peaks of specimens in Table 2, fitting relations with fitting coefficients of 0.9762 and 0.9995 can be obtained, respectively, as shown in

$$y = \frac{(91.82 - 34.12)}{1 + e^{(x-5.31)/2.03}} + 34.12, R^2 = 0.9762, \quad (3)$$

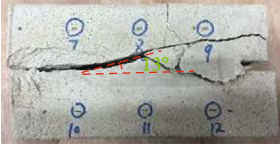

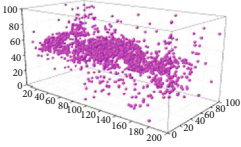
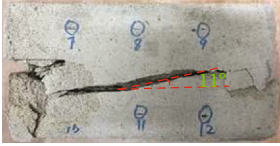

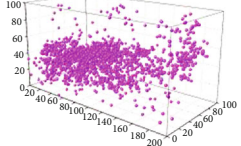
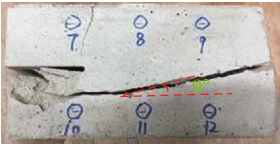

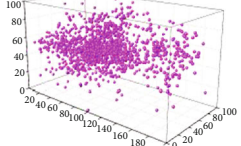


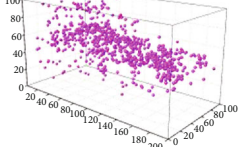
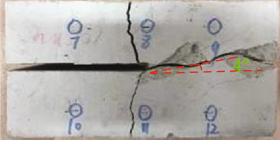
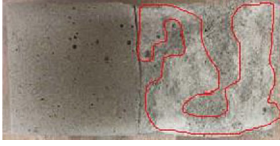
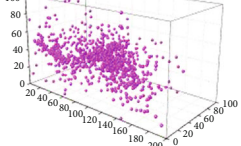
$$y = 32.24 + 0.47x - 2.36x^2 + 0.27x^3, R^2 = 0.9995. \quad (4)$$

The two fitting relations are drawn in the coordinate system, as shown in Figure 9. It can be seen that the AE count peaks of the specimens with different cracks have similar variation trends with the increase of the crack length, and both of them show a variation pattern which is an inverse "S" type. However, the curve of specimens with unilateral cracks is relatively flat and the value varied slowly, while the curve of specimens with bilateral cracks is much steeper than that of the former. Therefore, for the specimens with the same total crack length under the same test condition, the AE counting peak of specimens with unilateral cracks is higher than that of specimens with bilateral cracks.

3.4. Failure Characteristics. Table 3 shows the shear failure characteristics of specimens with different unilateral cracks. It can be seen that the specimens were not fractured along a flat surface. First, fracture cracks with different inclination angles were formed on the side of the specimens, as shown in the fracture angle column. The inclination angle of the fracture crack is 13°, 11°, 9°, 6°, and 4°, when the length of the crack is 2 cm, 4 cm, 6 cm, 8 cm, and 10 cm, respectively. This shows that the inclination angle of the crack decreases steadily with the increase of the crack length. Then, after shearing, the fracture surface of the specimens is rough and uneven, and the roughness of the fracture surface decreases with the increase of the crack length, as shown in the fracture surface column. After fracture, the roughness fracture surface resists further shear slip of rock blocks, which results in serious wear on the fracture surface. With the increase of the crack length, the proportion of the wear area on the fracture surface to the total fracture surface increases gradually. Finally, the fracture surface depicted by AE source locations is an uneven inclined surface, as shown in the AE source location column, which is in good agreement with the true fracture morphology of the specimens. The distribution of AE source locations is obviously asymmetric in the length direction of the specimen, mainly on the noncracked side, and the asymmetry becomes more obvious with the increase of the crack length. In addition, the number of AE sources decreases with the increase of the crack length, which indicates that the longer the crack, the less energy consumed when the specimen is fractured.

Table 4 shows the shear failure characteristics of specimens with different bilateral cracks. It can be seen that the shear failure characteristics of specimens with different bilateral cracks are very similar to those of specimens with different unilateral cracks. The difference is that two parallel fracture cracks are formed on the specimens when the lengths of the cracks are 0 cm and 2 cm, respectively. As two main fracture cracks appear, more AE locations are

TABLE 3: Failure mode of specimens with different unilateral cracks.

Crack length	Fracture angle	Fracture surface	AE source location
2 cm			
4 cm			
6 cm			
8 cm			
10 cm			

generated. Moreover, the inclination angle of the fracture crack is 20° , 16° , 14° , and 5° , when the length of the crack is 0 cm, 2 cm, 4 cm, and 6 cm, respectively. This shows that the inclination angle of the crack shows a nonuniform decreasing trend with the increase of the crack length.

4. Conclusions

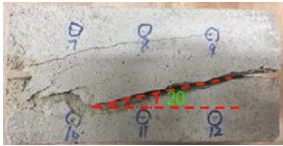

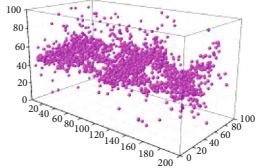
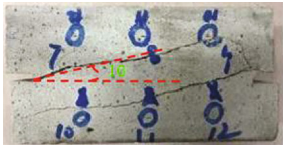
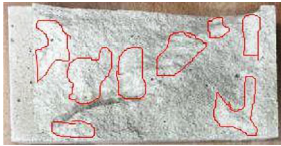
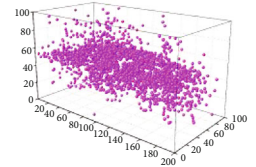
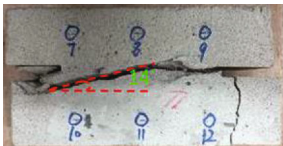

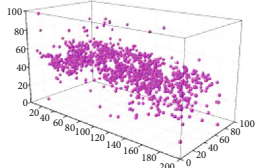
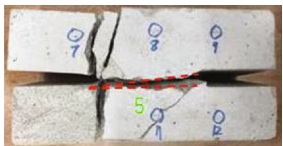

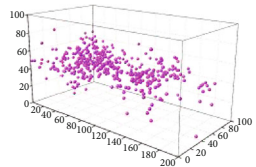
In this paper, laboratory shear tests were carried out to investigate the shear behavior of rock discontinuities with nonpersistent joints. The influence of the crack position and length on shear behavior is systematically observed based on the results. The following conclusions were reached:

- (1) Variation trends of the shear stress-displacement curves with different cracks are generally similar and have the same stage characteristics. When the crack length is relatively short, the elastic stage is prolonged, the peak shear strength decreases, and the shear displacement corresponding to peak shear strength and the residual shear strength increases with the increase of the crack length. When the crack length is relatively long, the elastic stage shortens, the

peak shear strength decreases, and the shear displacement corresponding to the peak shear strength increases with the increase of the crack length

- (2) The peak shear stress decreases with the increase of the crack length, and the decrease range of specimens with unilateral cracks is first increased and then decreased, while that of specimens with bilateral cracks is first decreased and then increased. Meanwhile, the shear strengths of the specimens with unilateral cracks are much higher than those of specimens with bilateral cracks. The shear strength is affected not only by the crack length, but also by the crack distribution. The influence of the distribution is more obvious when the total crack length is small
- (3) The peak of the AE count occurs when the shear stress drops sharply and a large amount of energy will be released at the moment. The AE count peaks of specimens with different cracks have a similar variation trend with the increase of the crack length, and both show a variation pattern which is an inverse "S" type. For the specimens with the same total crack

TABLE 4: Failure mode of specimens with different bilateral cracks.

Crack length	Fracture angle	Fracture surface	AE source location
0 cm			
2 cm			
4 cm			
6 cm			

length, the AE counting peak of specimens with unilateral cracks is higher than that of specimens with bilateral cracks

- (4) The inclination angle of the fracture decreases, the roughness of the fracture surface decreases, and the proportion of the wear area on the fracture surface increases gradually with the increase of the crack length. The distribution of AE source locations is obviously asymmetric, mainly on the noncracked side, and the asymmetry becomes more obvious with the increase of the crack length. The number of AE sources decreases with the increase of the crack length, which indicates that the longer the crack, the less the energy consumed

Data Availability

The data used to support the findings of this study are available from the corresponding author upon request.

Conflicts of Interest

The authors declare no conflict of interest.

Acknowledgments

This work is supported by the Shandong Provincial Natural Science Foundation (No. ZR2019BEE065), the Shandong

University of Science and Technology Graduate Innovation Fund (Nos. sskdyc190115 and sskdyc190232).

References

- [1] X. Wang, W. Yuan, Y. Yan, and X. Zhang, "Scale effect of mechanical properties of jointed rock mass: a numerical study based on particle flow code," *Geomechanics and Engineering*, vol. 21, no. 3, pp. 51–60, 2020.
- [2] W. Han, G. Li, Z. Sun, H. Luan, C. Liu, and X. Wu, "Numerical Investigation of a Foundation Pit Supported by a Composite Soil Nailing Structure," *Symmetry*, vol. 12, no. 2, p. 252, 2020.
- [3] P. Wang, L. Jiang, P. Zheng, G. Qin, and C. Zhang, "Inducing mode analysis of rock burst in fault-affected zone with a hard-thick stratum occurrence," *Environmental Earth Sciences*, vol. 78, no. 15, p. 467, 2019.
- [4] J. Fan, C. Jie, D. Jiang, A. Chemenda, J. Chen, and J. Ambre, "Discontinuous cyclic loading tests of salt with acoustic emission monitoring," *International Journal of Fatigue*, vol. 94, pp. 140–144, 2017.
- [5] B. Zheng and S. Qi, "A new index to describe joint roughness coefficient (JRC) under cyclic shear," *Engineering Geology*, vol. 212, pp. 72–85, 2016.
- [6] A. Fathi, Z. Moradian, P. Rivard, and G. Ballivy, "Shear mechanism of rock joints under pre-peak cyclic loading condition," *International Journal of Rock Mechanics and Mining Sciences*, vol. 83, pp. 197–210, 2016.
- [7] A. K. Shrivastava and K. S. Rao, "Physical modeling of shear behavior of infilled rock joints under CNL and CNS boundary

- Conditions,” *Rock Mechanics and Rock Engineering*, vol. 51, no. 1, pp. 101–118, 2018.
- [8] S. Mehrishal, M. Sharifzadeh, K. Shahriar, and J. Song, “An experimental study on normal stress and shear rate dependency of basic friction coefficient in dry and wet limestone joints,” *Rock Mechanics and Rock Engineering*, vol. 49, no. 12, pp. 4607–4629, 2016.
- [9] S. M. M. Niktabar, K. S. Rao, and A. K. Shrivastava, “Effect of rock joint roughness on its cyclic shear behavior,” *Journal of Rock Mechanics and Geotechnical Engineering*, vol. 9, no. 6, pp. 1071–1084, 2017.
- [10] Y. Cui, “Effect of joint type on the shear behavior of synthetic rock,” *Bulletin of Engineering Geology and the Environment*, vol. 78, no. 5, pp. 3395–3412, 2019.
- [11] H. K. Singh and A. Basu, “A comparison between the shear behavior of ‘real’ natural rock discontinuities and their replicas,” *Rock Mechanics and Rock Engineering*, vol. 51, no. 1, pp. 329–340, 2018.
- [12] Q. Jiang, B. Yang, F. Yan, C. Liu, Y. Shi, and L. Li, “New method for characterizing the shear damage of natural rock joint based on 3D engraving and 3D scanning,” *International Journal of Geomechanics*, vol. 20, no. 2, article 06019022, 2020.
- [13] V. Sarfarazi, A. Ghazvinian, W. Schubert, and M. Blumel, “Numerical simulation of the process of fracture of echelon rock joints,” *Rock Mechanics and Rock Engineering*, vol. 47, no. 4, pp. 1355–1371, 2014.
- [14] V. Sarfarazi, A. Ghazvinian, and W. Schubert, “Numerical simulation of shear behaviour of non-persistent joints under low and high normal loads,” *Periodica Polytechnica Civil Engineering*, vol. 60, no. 4, pp. 517–529, 2016.
- [15] X. Yang and W. Qiao, “Numerical investigation of the shear behavior of granite materials containing discontinuous joints by utilizing the flat-joint model,” *Computers and Geotechnics*, vol. 104, pp. 69–80, 2018.
- [16] H. Li, Z. Dong, Z. Ouyang, B. Liu, W. Yuan, and H. Yin, “Experimental investigation on the deformability, ultrasonic wave propagation, and acoustic emission of rock salt under triaxial compression,” *Applied Sciences*, vol. 9, no. 4, p. 635, 2019.
- [17] D. Zhang, S. Li, X. Bai, Y. Yang, and Y. Chu, “Experimental study on mechanical properties, energy dissipation characteristics and acoustic emission parameters of compression failure of sandstone specimens containing en echelon flaws,” *Applied Sciences*, vol. 9, no. 3, p. 596, 2019.
- [18] P. Rodríguez, P. B. Arab, and T. B. Celestino, “Characterization of rock cracking patterns in diametral compression tests by acoustic emission and petrographic analysis,” *International Journal of Rock Mechanics and Mining Sciences*, vol. 83, pp. 73–85, 2016.
- [19] Y. H. Li, J. P. Liu, X. D. Zhao, and Y. J. Yang, “Experimental studies of the change of spatial correlation length of acoustic emission events during rock fracture process,” *International Journal of Rock Mechanics and Mining Sciences*, vol. 47, no. 8, pp. 1254–1262, 2010.
- [20] J. Liu, Y. Li, S. Xu, S. Xu, and C. Jin, “Cracking mechanisms in granite rocks subjected to uniaxial compression by moment tensor analysis of acoustic emission,” *Theoretical and Applied Fracture Mechanics*, vol. 75, pp. 151–159, 2015.
- [21] F. Meng, H. Zhou, S. Li et al., “Shear behaviour and acoustic emission characteristics of different joints under various stress levels,” *Rock Mechanics and Rock Engineering*, vol. 49, no. 12, pp. 4919–4928, 2016.
- [22] G. Wang, X. Zhang, Y. Jiang, X. Wu, and S. Wang, “Rate-dependent mechanical behavior of rough rock joints,” *International Journal of Rock Mechanics and Mining Sciences*, vol. 83, pp. 231–240, 2016.
- [23] G. Wang, Y. Jiang, W. Wang, and T. Li, “Development and application of an improved numeric control shear-fluid coupled apparatus for rock joint,” *Rock and Soil Mechanics*, vol. 30, pp. 3200–3208, 2009.
- [24] X. Zhang, Q. Jiang, C. Na, W. Wei, and X. Feng, “Laboratory investigation on shear behavior of rock joints and a new peak shear strength criterion,” *Rock Mechanics and Rock Engineering*, vol. 49, no. 9, pp. 3495–3512, 2016.
- [25] Y. Jiang, Y. Wang, P. Yan, H. Luan, and Y. Chen, “Experimental investigation on the shear properties of heterogeneous discontinuities,” *Geotechnical and Geological Engineering*, vol. 37, no. 6, pp. 4959–4968, 2019.